Journal of Materials Chemistry C

Hybrid Schottky and Heterojunction Vertical β-Ga2O3 Rectifiers

Journal:	*Journal of Materials Chemistry C*
Manuscript ID	TC-ART-07-2024-003046.R1
Article Type:	Paper
Date Submitted by the Author:	10-Sep-2024
Complete List of Authors:	Li, Jian-Sian; National Taiwan University, Chemical Engineering Chiang, Chao-Ching; University of Florida, Department of Chemical Engineering Wan, Hsiao-Hsuan; University of Florida, Chemical Engineering Labed, Madani; Sejong University, Semiconductor Systems Engineering Park, Jang Hyeok; Sejong University, Department of Semiconductor Systems Engineering and Convergence Engineering for Intelligent Drone; Sejong University, Semiconductor Systems Engineering Rim, You Seung; Sejong University, School of Intelligent Mechatronics Engineering Yu, Meng-Hsun; National Yang Ming Chiao Tung University, Department of Electronics and Electrical Engineering Ren, Fan; University of Florida, Department of Chemical Engineering Liao, Yu-Te; National Yang Ming Chiao Tung University, Department of Electronics and Electrical Engineering Pearton, Stephen; Univ.Florida, MSE

Hybrid Schottky and Heterojunction Vertical β-Ga_2O_3 Rectifiers

Jian-Sian Li[1], Chiao-Ching Chiang[1], Hsiao-Hsuan Wan[1], Madani Labed [2,3], Jang Hyeok Park[2,3], You Seung Rim [2,3], Meng-Hsun Yu [4], Fan Ren[1], Yu-Te Liao[4] and Stephen J. Pearton[5]

[1]Department of Chemical Engineering, University of Florida, Gainesville, Florida 32611, USA

[2]Department of Semiconductor Systems Engineering and Convergence Engineering for Intelligent Drone, Sejong University, Seoul, Republic of Korea.

[3]Institute of Semiconductor and System IC, Sejong University, Seoul 05006, Republic of Korea

[4] Department of Electronics and Electrical Engineering, National Yang Ming Chiao Tung University, Hsinchu 30010, Taiwan.

[5]Department of Materials Science and Engineering, University of Florida, Gainesville, Florida 32611, USA

ABSTRACT

Junction Barrier Schottky design Ga_2O_3 rectifiers allow for a combination of low turn-on voltage and high breakdown voltage. Ni/Au/Ga_2O_3 Schottky rectifiers and NiO/Ga_2O_3 heterojunction rectifiers were fabricated on the same wafer and the percentage of the relative areas and diameters of each were varied from pure Schottky devices to pure heterojunction devices. The on-voltage increased from 0.6 V for Schottky rectifiers to 2.4 V for heterojunction rectifiers, with a monotonic decrease in forward current at fixed bias of 5V from 375 nA.cm^{-2} to 175 nA.cm^{-2}. Conversely, the breakdown voltage increased monotonically as the proportion of heterojunction area increased, from 1.2 kV for Schottky rectifiers to 6.2 kV for pure heterojunction devices. Breakdown mostly was initiated at the edge of the anode contact but could also occur at the transition region from the Schottky contact to NiO edge termination. The Baliga figure of merit

increased with both the relative percentage of area and diameter of the heterojunction contact from 0.2 GW.cm^{-2} to 3GW.cm^{-2}, while the energy loss during switching also increased from 2 to 3.9 W.cm^{-2}. These trends illustrate the trade-offs of Schottky versus pn junctions for the operation of Ga_2O_3 rectifiers.

CORRESPONDING AUTHORS: Stephen J. Pearton, spear@mse.ufl.edu; Madani Labed, madani95@sejong.ac.kr ; You Seung Rim youseung@sejong.ac.kr

Introduction

There is significant recent interest in development of Ga_2O_3 based rectifiers and transistors for advanced power electronic devices and RF amplifiers [1-7]. Their elevated critical electric field, coupled with reasonable transport characteristics and high permittivity, facilitates high-voltage operation within compact dimensions [8-13]. This characteristic mitigates parasitic capacitances and produces high switching efficiencies in applications such as power conversion in electric vehicles and smart grids [1-3, 12, 13]. Additionally, it enables the attainment of the requisite power densities and power added efficiencies in future 5G/6G wireless communications and radar systems [1-3]. There is also growing interest in their utilization in radiation-hardened applications, notably for space-borne systems [14].

Despite significant advancements in the bulk and epitaxial growth of the β-polytype of Ga_2O_3, devices fabricated from this material have yet to achieve their maximum theoretical performance, particularly at high voltages and frequencies [2,4]. Achieving this entails gaining a deeper understanding of breakdown and charge transport mechanisms, electron-hole recombination processes, and interactions with charged defects under specific operational conditions [15-18]. This necessitates comprehensive experimental studies as well as modeling and simulation support.

A significant advance in breakdown voltages for Ga_2O_3 based rectifiers has come from the development of NiO/Ga_2O_3 pn heterojunctions [19-27]. Breakdown voltages up to 13.5 kV were recently demonstrated in small diameter (100 μm) vertical NiO/Ga_2O_3 rectifiers and 7.2kV in large diameter (1 mm) devices [26]. These are both more than the theoretical 1D limit of performance of comparable GaN and SiC rectifiers, although those technologies are far more mature in terms of thermal management, defect control, reliability, surge robustness and packaging [1-4]. A promising approach is the Junction Barrier Schottky (JBS) diode, which integrates the beneficial

characteristics of Schottky Barrier Diodes (SBDs) and PiN diodes [1,4,8,12, 25]. The JBS diode features low conduction losses similar to SBDs in the on-state, while in the off-state, it exhibits improved leakage current and breakdown voltage akin to PiN diodes. This is achieved through a structure where a single anode forms a Schottky contact with the n-type drift layer and a connection with the p^+ region, promoting depletion into the drift region under reverse bias. This structural configuration involves embedding p^+ regions of NiO beneath the anode. Our structure deviates from traditional JBS structures by having the NiO deposited on the surface rather than embedded. During forward bias operation, the JBS diode behaves similarly to an SBD, where the Schottky portion conducts the current, though the specific on-resistance might increase due to reduced conduction area near the junction [1,4,8,12, 25]. Forward conduction is influenced by the geometry or cell pitch, with increased Schottky area enhancing current flow. In reverse bias, the electric field profile initially resembles that of an SBD, but upon reaching a certain reverse bias, the Schottky portion becomes fully depleted, resembling the field profile of a PiN diode and enhancing blocking capabilities.

There are still many more systematic studies of Ga_2O_3 rectifier design needed to advance this technology. In this work, we study the effect of systematically varying the relative area of Schottky and heterojunction rectifiers fabricated on the same wafer to understand the effect on forward turn-on voltage, reverse breakdown voltage, power figure of merit and switching losses.

Experimental

The rectifiers were fabricated on thick (~10 μm) lightly doped epitaxial layers grown by Halide Vapor Phase Epitaxy on heavily doped ($n \sim 8 \times 10^{18}$ cm^{-3}) bulk substrates with (001) orientation grown by the Edge- Defined Film-Fed technique. Ohmic contacts were formed on the backside of the wafers by deposition of e-beam evaporated Ti/Au. This was subsequently annealed

at 550 °C for 3 min. Both Schottky barrier diodes (SBD) pure heterojunction diodes (HJD)and JBS diodes were fabricated on the same wafer, with the schematic structure shown in **Figure 1**. A bilayer of Ni/Au was used for the Schottky contact and to make contact to the p^+NiO deposited by sputtering. Deposition conditions for the bilayer NiO have been reported previously [28]. In brief, this is done at low sputtering powers and the doping concentrations for the respective layers were 2.6 x 10^{18} cm^{-3} for the upper layer with a thickness of 10 nm, and 10^{18} cm^{-3} for the 10 nm lower layer, as controlled through the O_2 ratio during sputtering [28]. Thus, the hybrid JBS structure consists of an area with Schottky behavior and a different area where a heterojunction rectifier is formed. The ratio of the two areas was varied between the two extremes (100% Schottky or 100% heterojunction) by varying the diameter of the opening where the Schottky contact was made. This diameter was varied from 20-80 µm, while the diameter of the Ni/Au contact was held constant at 100 µm. All the devices were fabricated on a 1 cm x 1cm sample. The opening diameter of NiO varies. The percentage of the Schottky contact area was varied from 4-64%. Measurements from five devices of each structure were performed. The NiO/Ni/Au behaves as an Ohmic contact.

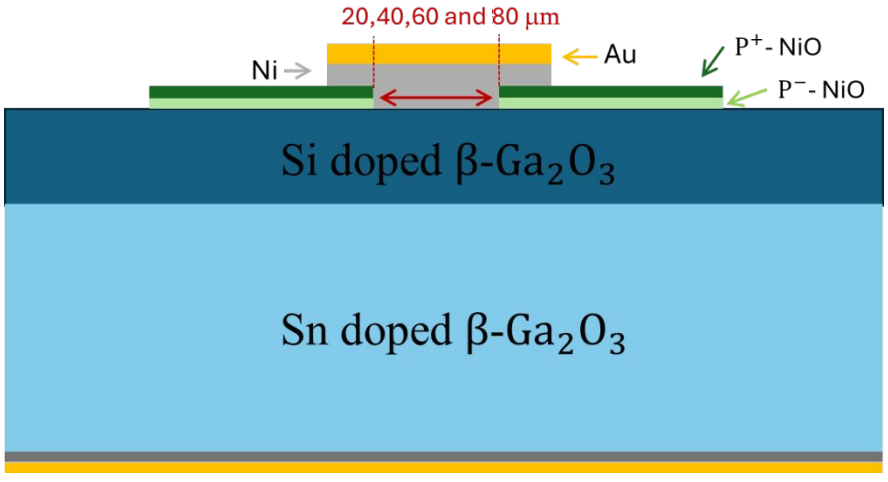

Figure 1. Schematic of the hybrid devices. The diameter of the Ni/Au Schottky contact on the Ga_2O_3 was increased from 20-80 µm, while holding the total diameter of the contact constant. This effectively varies the percentage of the device that has Schottky behavior relative to that which has NiO/Ga_2O_3 heterojunction behavior.

The carrier concentrations within the drift regions of the devices were quantified utilizing 1 MHz capacitance-voltage (C-V) measurements, with subsequent plotting of $1/C^2$-V data. **Figure 2** depicts the C-V and $1/C^2$-V plots corresponding to 10 µm thick drift layers, showing the carrier concentrations were $5.2x10^{15}$ cm^{-3} in the drift region.

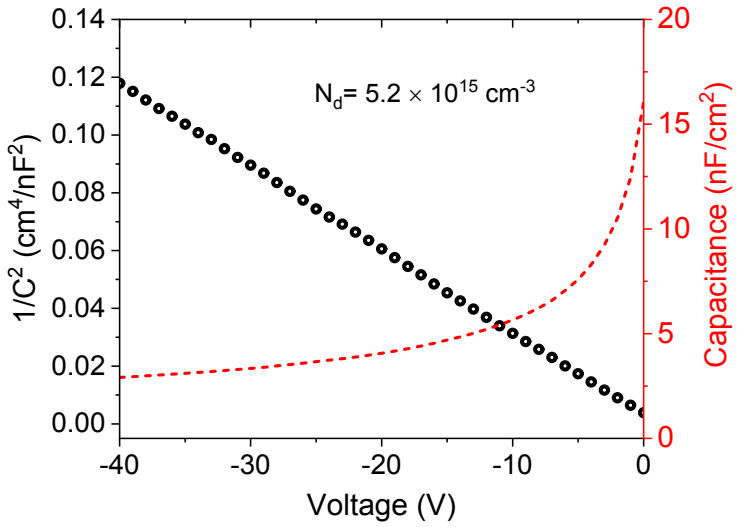

Figure 2. C-V and C^{-2}-V characteristics to extract doping in drift layer.

Current-voltage (I-V) characteristics were assessed under Fluorinert atmospheres at a temperature of 25°C, employing a Tektronix 371-B curve tracer in tandem with a Glassman high-voltage power supply. Low voltage forward and reverse current characteristics were analyzed using an Agilent 4156C parameter analyzer. The determination of the reverse breakdown voltage adhered to the conventional criterion, where reverse current density reached 0.1 A/cm^2. A mega-Ohm resistor was incorporated into the setup, and the resultant voltage drop across it was deducted.

Furthermore, prior to each breakdown test, contact integrity was ensured by conducting a forward sweep up to 5V, followed by a reverse sweep up to -100V, and confirming the I-V characteristics. On-resistance was derived from the voltage-current (dV/dI) derivative extracted from the I-V characteristics. Corrections were applied to compensate for the resistance contributed by external circuit components, encompassing cables, chuck, and probe, collectively amounting to 10 Ω, determined through I-V measurements while the cables, chuck, and probe were interconnected.

The dependence of forward current on perimeter to area ratio gives an indication of the relative contributions of surface and bulk current mechanisms [29]. We measured a range of parameters as a function of both the percentage area or diameter of the Schottky contact relative to the total anode contact area, including on-voltage (V_{on}), breakdown voltage (V_{br}) [30], Baliga's figure-of-merit (V_B^2/R_{ON}) and energy switching loss, defined as Energy loss = $D \bullet P_{on} + (1-D) \bullet P_{OFF} = D \bullet V_F$ (at 100A/cm^2) $\bullet$100 A/cm^2+ (1-D) $\bullet$100V$\bullet$ I(at-100V), where D is the duty cycle (we used 1%).

In addition, SILVACO TCAD simulations were performed to extract electric field and electron current density profiles [16]. This incorporates the necessary stress-dependent mobility and bandgap models, a high field saturation model, a trap-assisted Shockley-Read-Hall recombination model, a thermionic current model, a band gap narrowing model, and drift-diffusion and energy balance transport equations.

Results and Discussion

Figure 3 (a) shows the forward J-V characteristics and related R_{on} values for the range of hybrid devices examined. Five devices of each type were measured. The pure Schottky diodes have the highest forward current and lowest R_{on} values (~10 mΩ.cm^2) due to the lower effective barrier height compared to the heterojunction devices. The on-voltages could be derived from the slope of the linear J-A characteristics, shown in **Figure 3(b)**. These span from 0.75 V for Schottky

rectifiers to 2.3 to 2.4 V for pure heterojunction rectifiers. **Figure 3 (c)** shows the area dependence of V_{on} and forward current density at a fixed forward bias voltage of 5 V of the hybrid devices as a function of the Schottky contact area relative to the total area. The same data is shown in **Figure 3 (d)** as a function of the percentage of Schottky contact diameter relative to the total diameter of the hybrid devices. There is not a linear relationship of forward current in either case and this non-linear behavior can be explained by the effect of heterojunction thermionic emission of electrons from Ga_2O_3 to NiO as shows in simulation figures in addition to the recombination current. Since current is not directly proportional to either area or perimeter, both bulk and surface current contributions are present.

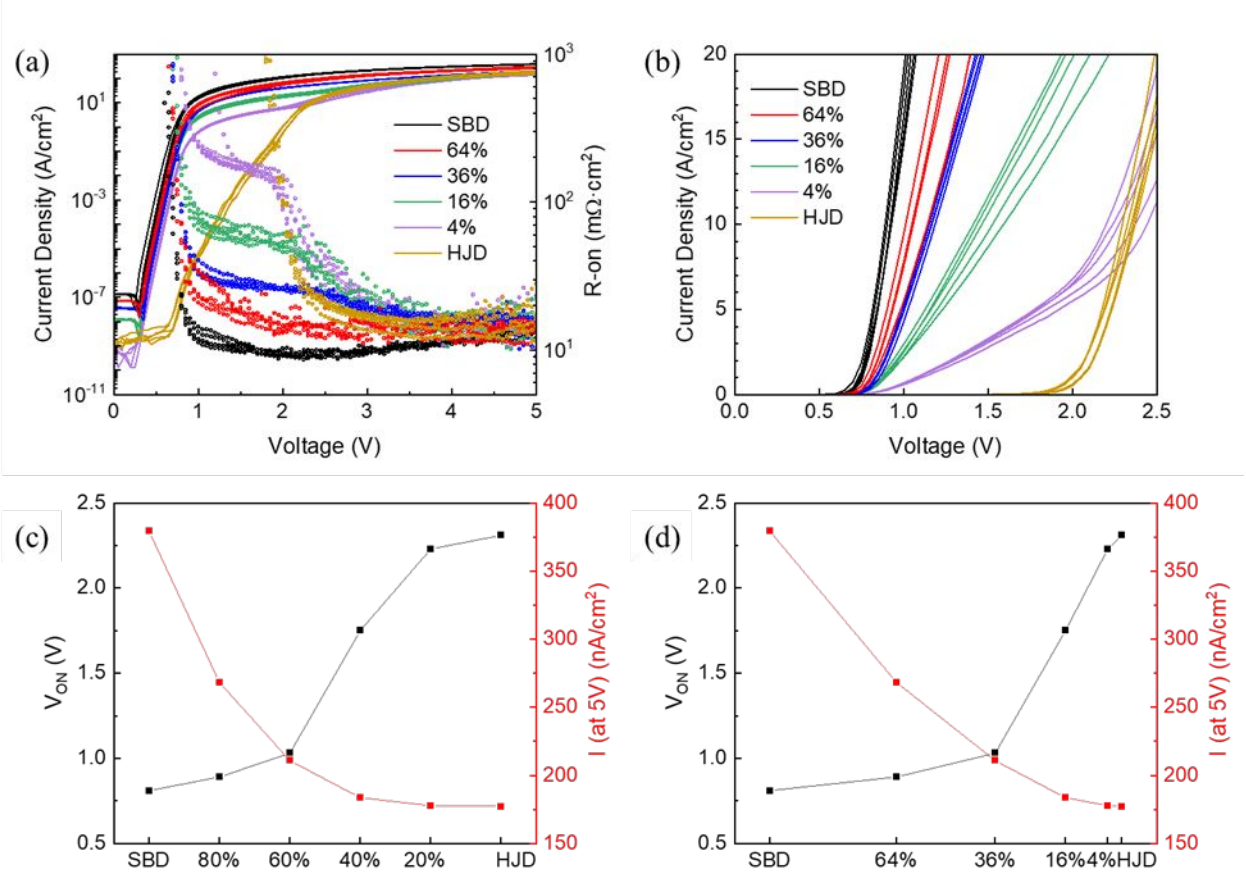

Figure 3. Forward current density plotted on a logarithmic scale (a) and a linear scale (b) as a function of bias for devices. (c) and (d) On-voltage and forward current at 5V bias for hybrid devices with varying percentages of the area and diameter of the Schottky contact respectively.

The nonlinear relationship between the on-voltage as a function of the Schottky contact area relative to the total area (**Figure 3 (c)**) or to the percentage of Schottky contact diameter relative to the total diameter (**Figure 3 (d)**) and forward current can be explained by the dominance of a new transport mechanism as the Schottky contact area decreases. The expected transport mechanism involves the transfer of electrons from β-Ga_2O_3 to NiO and then to the Ni contact as we will confirm using Silvaco TCAD. Due to the ultrathin NiO layers, different mechanisms are anticipated, with thermionic emission and tunneling being the most probable [16, 20, 25]. In addition, surface recombination in Ni/β-Ga_2O_3, with a lesser effect in NiO/β-Ga_2O_3, may significantly impact the linear behavior of the forward current at different Schottky contact areas due to the influence of electron traps in the β-Ga_2O_3 [31-35].

There is, as yet no direct measurement of the surface recombination velocity of β-Ga_2O_3 although numerous studies have shown the surface is easily disrupted by dry etching steps or thermal degradation [31-35]. Bulk leakage contributions may originate from stacking faults, polycrystalline inclusions and dislocations present in the drift region [15, 32- 39]. Furthermore, as shown in **Figure 3 (b)**, we observed transitions in the slopes of the linear regions at high forward voltages in the 16% and 4% hybrid junction diodes. To understand the underlying reasons for this behavior, we utilized SILVACO TCAD simulations. First, as shown in Figure 4(a) the simulated current density for all devices, we noticed the formation of the transition slopes for the cases 16 % and 4 % hybrid junction diodes which highly agree with the measured behavior. However there

are minor deviation between simulations and measurements as shown in **Figure 4 (b)**. This small deviation explained by the effect of interfacial states in NiO/β-Ga_2O_3 interface.

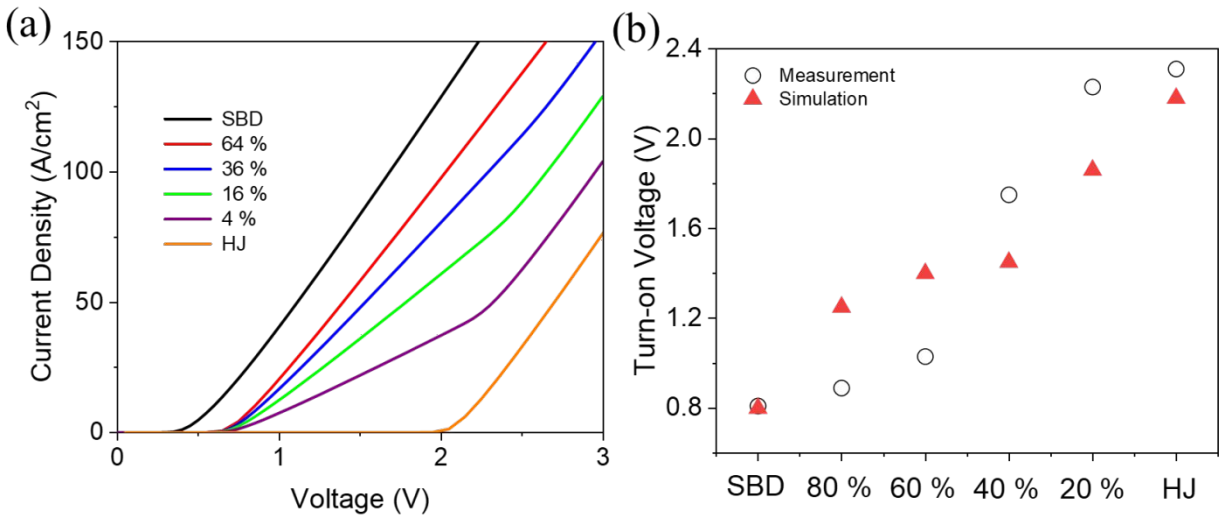

Figure 4. (a) Simulated forward current density plotted on a linear scale and (b) Simulated on-voltage for hybrid devices with varying percentages of the area and diameter of the Schottky contact and compared with measurement.

Now, to deeply understand the reason of the observed transitions in the slopes of the linear regions at high forward voltages in the 16% and 4% hybrid junction diodes, we compared the electron current density under +1 V and +4 V for both 16% and 4% hybrid junction diodes with that of the 64% hybrid junction diode.

As shown in **Figure 5**, at +1 V, the direct thermionic emission of electrons from β-Ga_2O_3 to the Ni Schottky contact dominates for the 16%, 4%, and 64% hybrid junction diodes. However, when the applied voltage is increased to +4 V, a new mechanism appears in the 16% and 4% hybrid junction diodes. This mechanism involves the transfer of electrons from β-Ga_2O_3 to NiO, and subsequently to the Ni contact, by thermionic emission. In contrast, this mechanism is less

dominant in the 64% diode due to the thicker rings and reduced contact area between NiO and Ni. Thus, we conclude that the transitions in the slopes of the linear regions at high forward voltages in the 16% and 4% hybrid junction diodes are attributed to the transition of electrons from β-Ga_2O_3 to NiO and then to the Ni contact by thermionic emission. In addition, this confirms the reason for the nonlinear behavior of the forward current at 5V at different Schottky contact areas as we discussed in **Figure 3 (c).** This behavior in electron flow also explains the non-linear variation of the V_{on} with the Schottky contact area. For SBDs covering less than 60% of the contact area, we observed that the V_{on} value closely matches that of a standard SBD. This can be attributed to the dominant thermionic emission of electrons from the β-Ga_2O_3 to the Ni contact. However, as the SBD area decreases and the HJ area increases, a new dominant process influences the V_{on} by the electrons emission from β-Ga_2O_3 to NiO, and subsequently to the Ni contact.

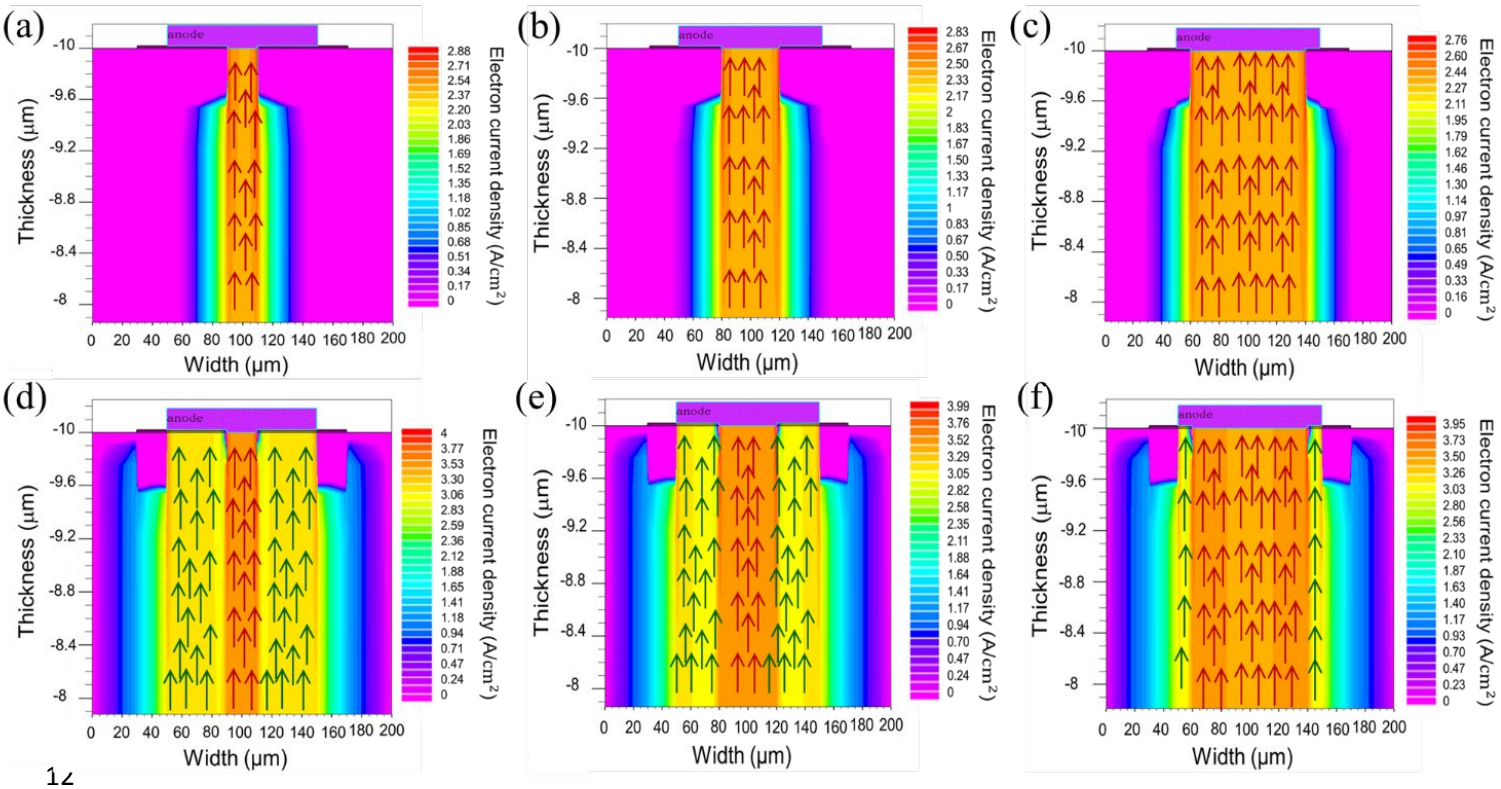

Figure 5. Electron current density (log scale) for hybrid junction diodes: (a) 4%, (b) 16%, and (c) 64% under 1V; (d) 4%, (e) 16%, and (f) 64% under 4V.

The reverse breakdown characteristics from the set of devices are shown in **Figure 6(a)**. The breakdown voltage (V_{br}) increased monotonically as the proportion of heterojunction area increased, from 1.2 kV for Schottky rectifiers to 6.2 kV for pure heterojunction devices. The same trend was seen in the low bias (≤ 100V) reverse J-V characteristics of **Figure 6 (b)**. **Figure 6 (c)** shows the area dependence of V_{br} and reverse current density at a fixed bias voltage of -100 V of the hybrid devices as a function of the Schottky contact area relative to the total area. The same data is shown in **Figure 6 (d)** as a function of the percentage of Schottky contact diameter relative to the total diameter of the hybrid devices. The relationship between breakdown voltage is relatively linear with both area and diameter over parts of the range investigated, with the V_{br} being linear with percentage area until pure HJDs and for hybrid devices other than pure SBDs. These trends may be an indication that surface effects predominate for Schottky contact devices whereas bulk effects are more important for heterojunction rectifiers. This is reasonable, since in the latter, the NiO would help screen surface states [5, 40-46]. The linear dependence of the V_{br} on the Schottky contact area relative to the total area can be explained by the shift in the electric field from the Ni/Ga_2O_3 edge in the SBD to the NiO/Ga_2O_3 edge in the HJ. This shift in the electric field distribution plays a crucial role in controlling the breakdown voltage. As the Schottky contact area decreases, the electric field becomes more concentrated at the NiO/Ga_2O_3 interface, which in turn affects the V_{br}. This shifting behavior offers a way to finely tune and control the breakdown voltage values by adjusting the relative size of the Schottky contact area.

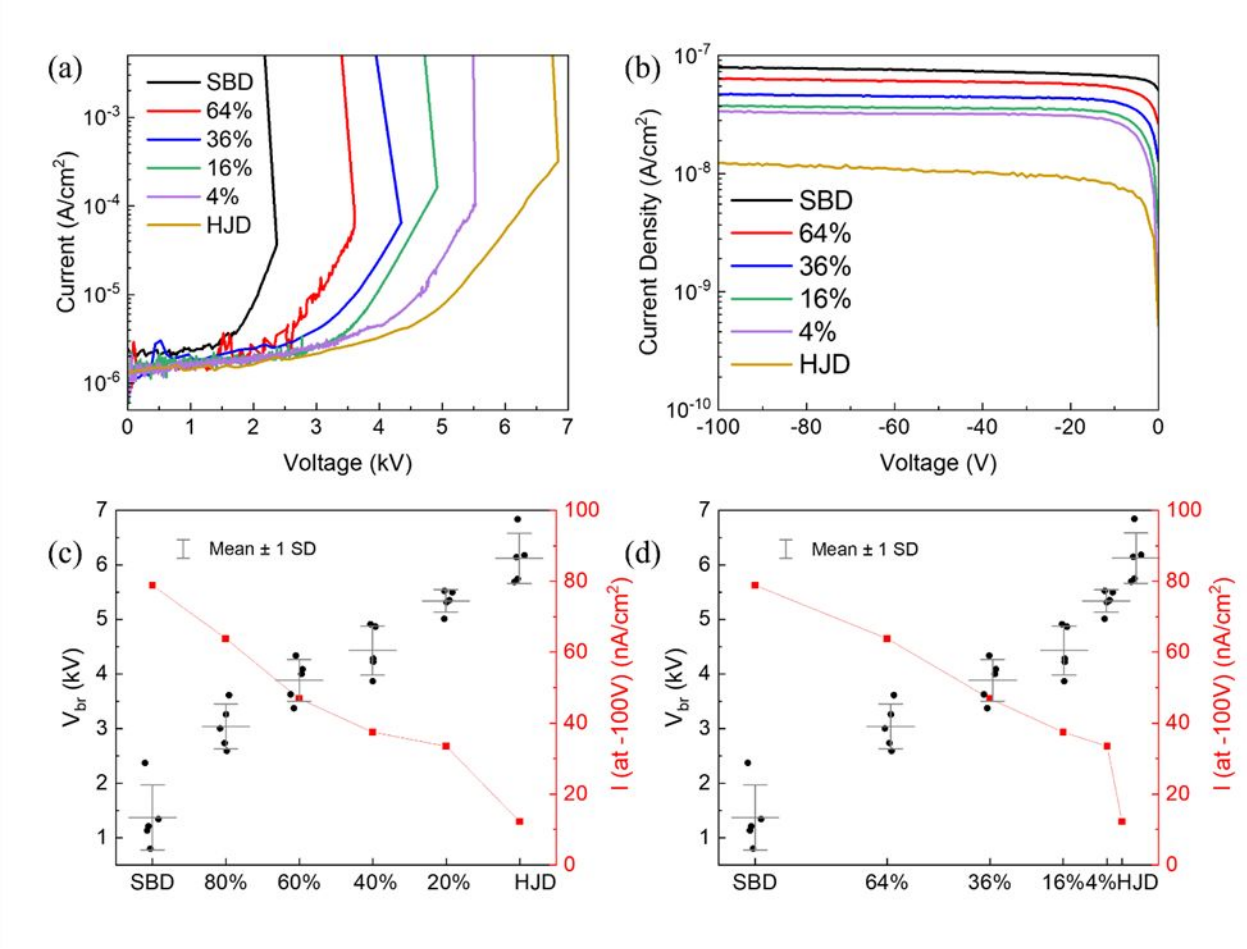

Figure 6. Reverse J-V characteristics at high bias (a) and low bias (b) for devices with varying percentages of the Schottky contact diameter. Breakdown voltage (c) and reverse current at -100V bias (d) for devices with different areas and diameters of the Schottky contact within the hybrid devices.

Breakdown mostly was initiated at the edge of the anode contact but could also occur at transition region from the Schottky contact to NiO edge termination. This is seen in the optical images of **Figure 7**. When we purposely drove the devices to failure at their breakdown voltage, pits were observed in the high field regions at the edges of the respective contact regions, either the edge of the Ni/Au anode or at the edge of the Schottky contact contained within that region.

This occurred in SBD at the edge of the metal contact and shifted to the edge of the NiO as the percentage of HJD area increased. For the hybrid JBS devices, the pits were located between the inner and outer edges of the NiO rings, depending on the distance between the metal edge and the NiO edges. For the 64% diode, the pit was located on the inner edge of the NiO, which might be due to it being closer to the metal edge. With a thicker NiO ring, it shifted to the outer side. In addition, we always observed that the pits in the center occurred before the ones on the edge. They were formed around the current density of 10 uA/cm^2.

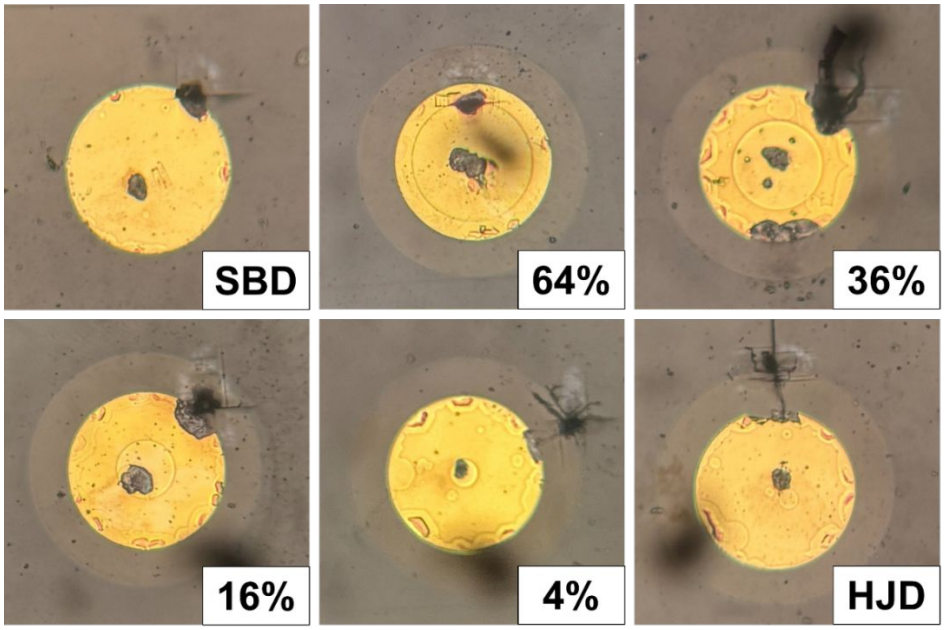

Figure 7. Optical images after reverse breakdown of the hybrid devices with varying percentages of the area of the Schottky contact relative to the total area.

The exact breakdown mechanism in Ga_2O_3 is still not established [12,20,26]. While avalanche failure at the high fields near the contact periphery is the usual cause in rectifiers of other wide bandgap semiconductors, is not clear what happens with Ga_2O_3, which has a significant component of ionicity to its bonds [48-50]. When impact ionization is the breakdown mechanism, this would be

characterized by a positive temperature dependence of breakdown on temperature [51]. In most previous materials, like SiC and GaN, this is only observed after many years of device and materials development to reduce defect density [33]. It has not been observed yet in Ga_2O_3 [12,26]. Even more importantly, it is suggested that since Ga_2O_3 has a large component of ionicity in its bonds [47-49], it may not breakdown by impact ionization, but more like an oxide, where direct bond-breaking occurs [50]. That would mean that the models for estimating Ecrit from breakdown voltages would not apply to Ga_2O_3. The degree of ionicity in Ga_2O_3 can be estimated based on the electronegativity difference between the atoms involved in the bonding. Ga is a metal, and O is a nonmetal. To calculate the degree of ionicity, one uses the Pauling scale of electronegativity [51]. The electronegativity of Ga is around 1.81, and the electronegativity of O is around 3.44 [51]. The electronegativity difference (ΔEN) between Ga and O in Ga_2O_3 e is: ΔEN = Electronegativity of O - Electronegativity of Ga = 3.44 - 1.81 = 1.63. When the electronegativity difference is greater than 1.7, the bond is considered predominantly ionic. In this case, the electronegativity difference is significant, indicating that the Ga-O bonds in Ga_2O_3 have a significant degree of ionicity.

Another expected breakdown mechanism, especially for type II heterojunctions, is the Zener breakdown mechanism. This phenomenon occurs when the reverse voltage applied across the diode exceeds a critical value, leading to a significant increase in reverse current [52]. This process is primarily driven by the strong electric field in the depletion region. For example, the NiO/Ga_2O_3 heterojunction exhibits type II behavior [12], which may facilitate the tunneling of electrons from the valence band of the p-type NiO to the conduction band of the n-type Ga_2O_3. In type II heterojunctions, the conduction band minimum of the n-type material is at a higher energy level than the valence band maximum of the p-type material, which enhances this tunneling process [52].

To understand the breakdown mechanism, electric field profiles for hybrid devices with varying percentages of the area of the Schottky contact relative to the total area were extracted using Silvaco TCAD. As we can see in **Figure 8(a)** and in the inset of **Figure 8 (a)**, the electric field peak is located at the edge of the Schottky barrier diode, and this agrees with the observed pits in the optical image. Then with decreasing Schottky contact area relative to the total area, we noticed that there are three formed peaks. The first peak is located in the inner edges of the NiO ring and the second peak in the outer edges of the NiO ring and other peak in the edge of NiO/Ga_2O_3 as shown in **Figures 8 (b)-(f)** and in the inset of **Figures 8 (b)-(f).** As shown in the insets of **Figure 8**, with the decreasing Schottky contact area relative to the total area, the electric field intensity at the surface of Ga_2O_3 near the outer edge of NiO increases significantly. This effect is especially pronounced in the case of the NiO/Ga_2O_3 heterojunction (approximately ~10^7 V/cm), confirming the observed pits in all cases. Note that the field distributions in the Ga_2O_3 under the contact are relatively uniform, The primary reason for this is the small thickness of the NiO layers used. When thicker layers (> 50 nm) are used, there is a larger extent of the field in the Ga_2O_3, leading to multiple peaks in the field distribution, as reported previously [25, 36].

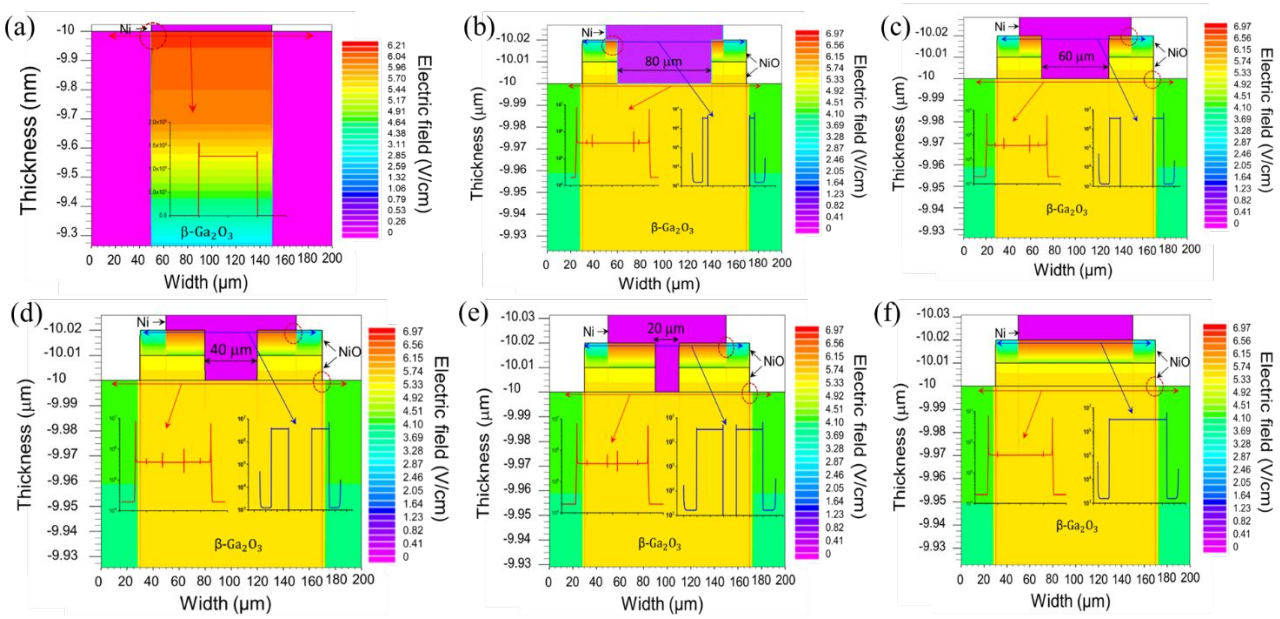

Figure 8. Electric field profiles for (a) Schottky diode, (b) 64%, (c) 36%, (d) 16%, and (e) 4% percentages of the area of the Schottky contact relative to the total area, and (f) NiO/Ga_2O_3 heterojunction. The insets show cutlines of the electric field at the surface of Ga_2O_3 and near the inner and outer edges of the NiO rings for each case under high reverse voltage.

As shown in **Figure 9**, the extracted electric field peak from the measurements exhibits a linear dependence on the Schottky contact relative to the total area, which is derived from the breakdown voltage value ($E_{Peak} = V_{br}/d$, where d = 10 μm (epitaxial film thickness)). As previously discussed, the electric field peak shifts from the Ni/Ga_2O_3 edge in the case of the SBD to the NiO/Ga_2O_3 edge in the case of the HJ. Simulated electric field peaks, extracted from the inset of **Figure 8**, also occur at the Ni/Ga_2O_3 and NiO/Ga_2O_3 edges.

When comparing the simulations with the measurements, we observed that for the SBD, the simulated electric field peak values closely align with those extracted from the measurements. As the Schottky contact relative to the total area decreases, the electric field peak located at the Ni/

Ga_2O_3 edge also decreases. The simulated values for the cases of 80%, 60%, and 40% Schottky contact area show strong agreement with the measured values at the Ni/Ga_2O_3 edge. However, when the Schottky contact area is reduced to 20%, we observed that the simulated electric field peak extracted from the NiO/Ga_2O_3 edge closely matches the value obtained from the measurements.

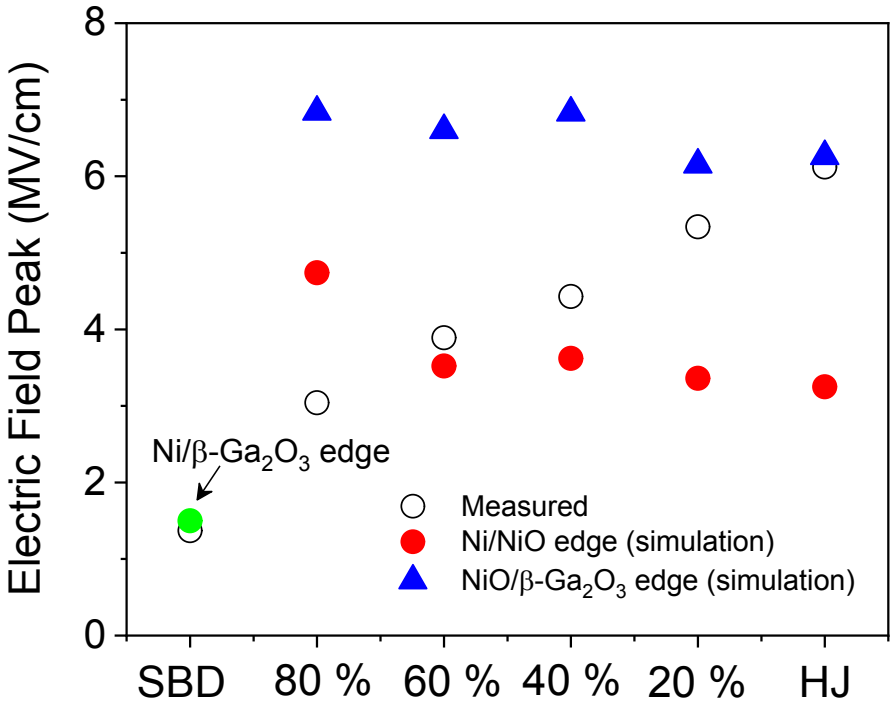

Figure 9. Comparison of the electric field peak extracted from measurements with simulated values at both the Ni/Ga_2O_3 and NiO/Ga_2O_3 edges.

Now, **Figure 10 (a)** shows the area dependence of the Baliga figure of merit and energy loss during switching of the hybrid devices as a function of the Schottky contact area relative to the total area. The same data is shown in **Figure 10(b)** as a function of the percentage of Schottky contact diameter relative to the total diameter of the hybrid devices. The power figure of merit scales almost linearly with device diameter, reflecting the trend of breakdown voltage.

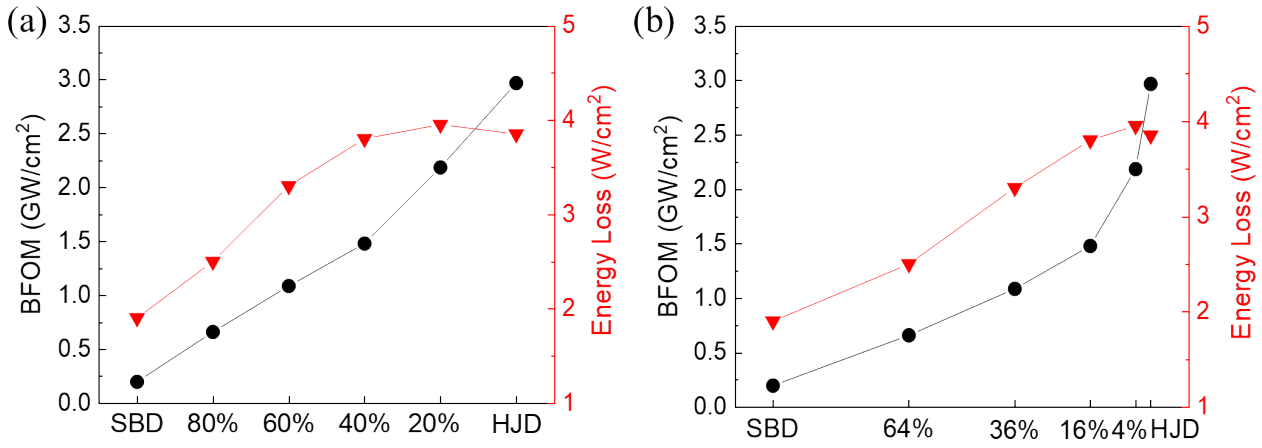

Figure 10. Baliga figure of merit and energy loss for hybrid devices with varying percentages of the area (a) or diameter (b) of the Schottky contact relative to the total area or diameter.

The turn-on voltage in rectifiers causes a reduction in efficiency and increased thermal losses [11,41,42]. Apart from the JBS rectifiers described here, other configurations that produce a reduced surface electric field at the anode and reduced increase in turn-on voltage include trench-Schottky barrier diodes, trench-MOS barrier diodes and metal-dielectric-semiconductor (MDS) diodes employing high permittivity dielectrics and negative conduction band offsets [11,41.42]. **Figure 11** summarizes the trade-off between breakdown voltage and Von reported recently from various groups [20- 27, 36-40]. For comparison, a commercially available SiC JBS rectifier has a V_{ON} near 1V and a breakdown field of ~2.5 MV/cm [12]. The higher breakdown fields of Ga_2O_3 do come at the cost of higher V_{ON}. Recent work on incorporating interlayers of TiN have shown the ability to tune the V_{ON}-V_B tradeoff [42].

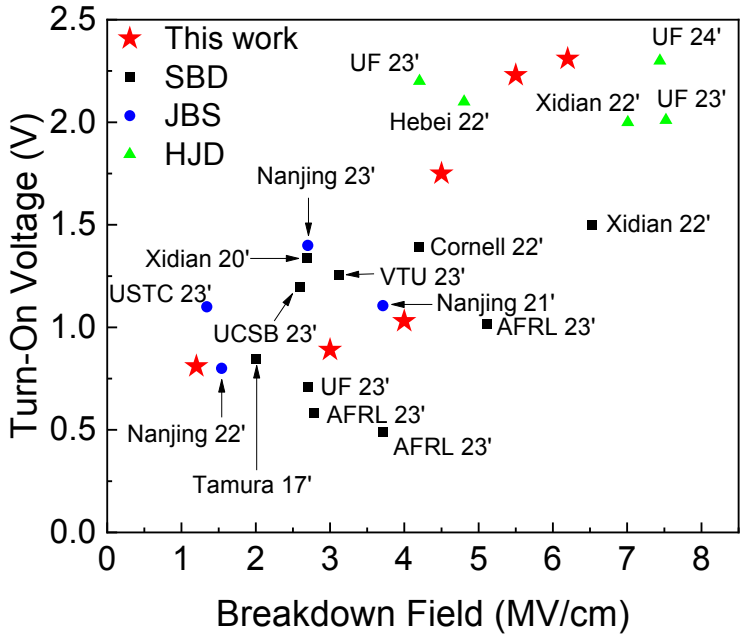

Figure 11. Summary of V_{on} results as a function of breakdown field in various types of vertical geometry Ga_2O_3 rectifiers reported by various groups.

Summary and Conclusions

The incorporation of NiO as a p-layer to provide JBS or heterojunction rectifiers, or as an edge termination material, significantly improves the breakdown voltage and lowers reverse leakage current [20-26, 36-42]. However, this also leads to higher turn-on voltage and switching losses. The trends in various device parameters for hybrid Schottky/heterojunction Ga_2O_3 rectifiers were examined as a function of the ratio of area or diameter of the Schottky contact relative to the total device area or perimeter. Schottky rectifiers have lower turn-on voltages but lower breakdown voltages relative to the heterojunction devices. Breakdown still occurs mostly at the anode edge, but in some cases, can also occur at the internal metal contact boundary in hybrid devices. Continued optimization of the edge termination [12] and switching characteristics [41] are still

needed to establish the operating conditions under which Ga_2O_3 rectifiers will have advantages over SiC.

Authors Contributions

Jian-Sian Li; Conceptualization (equal); Data curation (equal); Formal analysis (equal); Investigation (equal); Methodology (equal), Writing – original draft (equal)

Chiao-Ching Chiang; Conceptualization (equal); Data curation (equal); Formal analysis (equal); Investigation (equal); Methodology (equal), Writing – original draft (equal)

Hsiao-Hsuan Wan; Conceptualization (equal); Data curation (equal); Formal analysis (equal); Investigation (equal); Methodology (equal), Writing – original draft (equal)

Madani Labed; Conceptualization (equal); Data curation (equal); Formal analysis (equal); Investigation (equal); Methodology (equal), Writing – original draft (equal)

Jang Hyeok Park; Conceptualization (equal); Data curation (equal); Formal analysis (equal); Investigation (equal); Methodology (equal), Writing – original draft (equal)

You Seung Rim; Conceptualization (equal); Data curation (equal); Formal analysis (equal); Investigation (equal); Methodology (equal), Writing – original draft (equal)

Meng-Hsun Yu; Conceptualization (equal); Data curation (equal); Formal analysis (equal); Investigation (equal); Methodology (equal), Writing – original draft (equal)

Fan Ren; Conceptualization (equal); Data curation (equal); Formal analysis (equal); Investigation (equal); Methodology (equal), Writing – original draft (equal)

Yu-Te Liao

Stephen J. Pearton; Conceptualization (equal); Data curation (equal); Formal analysis (equal); Investigation (equal); Methodology (equal), Writing – original draft (equal)

Authors Contributions

Declarations

The authors have no conflicts to disclose.

Acknowledgments

The work at UF was performed as part of Interaction of Ionizing Radiation with Matter University Research Alliance (IIRM-URA), sponsored by the Department of the Defense, Defense Threat Reduction Agency under award HDTRA1-20-2-0002. The content of the information does not necessarily reflect the position or the policy of the federal government, and no official endorsement should be inferred. The work at Sejong University was supported by the Korea Institute for Advancement of Technology (KIAT) grant funded by the Ministry of Trade, Industry & Energy (MOTIE) in Korea (Project ID: P0012451, The Competency Development Program for Industry Specialists) and also supported by the MSIT(Ministry of Science and ICT), Korea, under the ITRC(Information Technology Research Center) support program (IITP-2024-RS-2024-00437494) supervised by the IITP(Institute for Information & Communications Technology Planning & Evaluation). The authors at National Yang Ming Chiao. Tung University would like to acknowledge the National Science and Technology Council, Taiwan, for their financial support under Grant No. NSTC 112-2628-E-A49-015.

Data Availability

The data supporting this article have been included as part of the Supplementary Information.

References

1. Mingfei Xu, Dawei Wang, Kai Fu, Dinusha Herath Mudiyanselage, Houqiang Fu, Yuji Zhao, A review of ultrawide bandgap materials: properties, synthesis and devices, Oxford Open Materials Science, 2, 2022, itac004 (2022) https://doi.org/10.1093/oxfmat/itac004 \

2. Kelly Woo, Zhengliang Bian, Maliha Noshin, Rafael Perez Martinez, Mohamadali Malakoutian, Bhawani Shankar and Srabanti Chowdhury, From wide to ultrawide-bandgap semiconductors for high power and high frequency electronic devices, J. Phys. Mater. 7, 022003 (2024), DOI 10.1088/2515-7639/ad218b

3. S. J. Pearton, Jiancheng Yang, Patrick H. Cary, F. Ren, Jihyun Kim, Marko J. Tadjer, Michael A. Mastro; A review of Ga_2O_3 materials, processing, and devices. Appl. Phys. Rev. 5, 011301 (2018). https://doi.org/10.1063/1.5006941

4. Y. He, F. Zhao, B. Huang, T. Zhang and H. Zhu, A Review of β-Ga_2O_3 Power Diodes. Materials, 17, 1870 (2024). https://doi.org/10.3390/ma17081870

5. Jincheng Zhang, Pengfei Dong, Kui Dang, Yanni Zhang, Qinglong Yan, Hu Xiang, Jie Su, Zhihong Liu, Mengwei Si, Jiacheng Gao, Moufu Kong, Hong Zhou and Yue Hao, Ultra-wide bandgap semiconductor Ga_2O_3 power diodes. Nat Commun, **13**, 3900 (2022). https://doi.org/10.1038/s41467-022-31664-y

6. F. Zhou, H. Gong, M. Xiao, Yunwei Ma, Zhengpeng Wang Xinxin Yu, Li Li, Lan Fu, Hark Hoe Tan, Yi Yang, Fang-Fang Ren, Shulin Gu, Youdou Zheng, Hai Lu, Rong Zhang, Yuhao Zhang and Jiandong Ye, An avalanche-and-surge robust ultrawide-bandgap heterojunction for power electronics, Nat Commun **14**, 4459 (2023). https://doi.org/10.1038/s41467-023-40194-0

7. T. Oishi, K. Urata, M. Hashikawa, K. Ajiro and T. Oshima, Microwave Power Rectification Using β -Ga_2O_3 Schottky Barrier Diodes, IEEE Electron Device Letters, 40, 1393 (2019), doi: 10.1109/LED.2019.2931793

8. J. Chen, X. Du, Q. Luo, X. Zhang, P. Sun and L. Zhou, A Review of Switching Oscillations of Wide Bandgap Semiconductor Devices, IEEE Transactions on Power Electronics, 35, 13182 (2020), doi: 10.1109/TPEL.2020.2995778

9. Y. Qin, B. Albano, J. Spencer, J. S. Lundh, B. Wang, C. Buttay, M. Tadjer, C. DiMarino, and Y. Zhang, Thermal management and packaging of wide and ultra-wide bandgap power devices: a review and perspective, J. Phys. D: Appl. Phys., 56, 093001 (2023). DOI 10.1088/1361-6463/acb4ff

10. Zhe Cheng, Samuel Graham, Hiroshi Amano, David G. Cahill; Perspective on thermal conductance across heterogeneously integrated interfaces for wide and ultrawide bandgap electronics. Appl. Phys. Lett. 120, 030501(2022). https://doi.org/10.1063/5.0077039

11. F. Wilhelmi, S. Kunori, K. Sasaki, A. Kuramata, Y. Komatsu and A. Lindemann, Packaged β -Ga_2O_3 Trench MOS Schottky Diode With Nearly Ideal Junction Properties, in IEEE Transactions on Power Electronics, 37, 3737 (2022), doi: 10.1109/TPEL.2021.3122902.

12. Andrew J. Green, James Speck, Grace Xing, Peter Moens, Fredrik Allerstam, Krister Gumaelius, Thomas Neyer, Andrea Arias-Purdue, Vivek Mehrotra, Akito Kuramata, Kohei Sasaki, Shinya Watanabe, Kimiyoshi Koshi, John Blevins, Oliver Bierwagen, Sriram Krishnamoorthy, Kevin Leedy, Aaron R. Arehart, Adam T. Neal, Shin Mou, Steven A. Ringel, Avinash Kumar, Ankit Sharma, Krishnendu Ghosh, Uttam Singisetti, Wenshen Li, Kelson Chabak, Kyle Liddy, Ahmad Islam, Siddharth Rajan, Samuel Graham, Sukwon Choi, Zhe

Cheng, Masataka Higashiwaki; β-Gallium oxide power electronics. APL Mater. 10, 029201(2022). https://doi.org/10.1063/5.0060327

13. A. K. Morya, Matthew C. Gardner, Bahareh Anvari, Liming Liu, Alejandro G. Yepes, Jesús Doval-Gandoy and Hamid A. Toliyat, Wide Bandgap Devices in AC Electric Drives: Opportunities and Challenges, IEEE Transactions on Transportation Electrification, 5, 3 (2019), doi: 10.1109/TTE.2019.2892807.

14. Xinyi Xia, Jian-Sian Li, Ribhu Sharma, Fan Ren, Md Abu Jafar Rasel, Sergei Stepanoff, Nahid Al-Mamun, Aman Haque, Douglas E Wolfe, Sushrut Modak, Leonid Chernyak, Mark E Law, Ani Khachatrian, Stephen J Pearton, Radiation damage in the ultra-wide bandgap semiconductor Ga_2O_3, ECS J. Solid State Science and Technol, 11, 095001 (2022), DOI 10.1149/2162-8777/ac8bf7

15. Sayleap Sdoeung, Kohei Sasaki, Satoshi Masuya, Katsumi Kawasaki, Jun Hirabayashi, Akito Kuramata, Makoto Kasu; Stacking faults: Origin of leakage current in halide vapor phase epitaxial (001) β-Ga_2O_3 Schottky barrier diodes. Appl. Phys. Lett. 118, 172106 (2021). https://doi.org/10.1063/5.0049761

16. Madani Labed, Nouredine Sengouga, Chowdam Venkata Prasad, Mohamed Henini, You Seung Rim, On the nature of majority and minority traps in β-Ga_2O_3: A review, Materials Today Physics,36, 101155 (2023), https://doi.org/10.1016/j.mtphys.2023.101155.

17. W. Li, K. Nomoto, Z. Hu, D. Jena and H. G. Xing, Guiding Principles for Trench Schottky Barrier Diodes Based on Ultrawide Bandgap Semiconductors: A Case Study in Ga_2O_3, IEEE Transactions on Electron Devices, 67, 3938 (2020), doi: 10.1109/TED.2020.3003292.

18. Saurav Roy, Arkka Bhattacharyya, Carl Peterson, Sriram Krishnamoorthy; 2.1 kV (001)-β-Ga_2O_3 vertical Schottky barrier diode with high-k oxide field plate. Appl. Phys. Lett. 122, 152101 (2023). https://doi.org/10.1063/5.0137935

19. Y. Kokubun, S. Kubo and S. Nakagomi, All-oxide p–n heterojunction diodes comprising p-type NiO and n-type β-Ga_2O_3. Appl Phys Express, 9, 091101 (2016).

20. Xing Lu, Yuxin Deng, Yanli Pe, Zimin Chen and Gang Wang, Recent advances in NiO/Ga_2O_3 heterojunctions for power electronics J. Semicond. 44, 061802 (2023), DOI 10.1088/1674-4926/44/6/061802

21. C. Liao, X. Lu, T. Xu, P. Fang, Y. Deng, H. Luo, Z. Wu, Z. Chen, J. Liang, Y. Pei and G. Wang, Optimization of NiO/β-Ga_2O_3 heterojunction diodes for high-power application. IEEE Transactions on Electron Devices, 69, 5722 (2022). doi 10.1109/TED.2022.3200642

22. P. Dong, J. Zhang, Q. Yan, Z. Liu, P. Ma, H. Zhou and Y. Hao, 6 kV/3.4 mΩ· cm^2 vertical β-Ga_2O_3 Schottky barrier diode with $BV^2/R_{on,\,sp}$ performance exceeding 1-D unipolar limit of GaN and SiC. IEEE Electron Device Letters, 43, 765 (2022). Digital Object Identifier 10.1109/LED.2022.3160366

23. F. Zhou, H. Gong, W. Xu, X. Yu, Y. Xu, Y, Yang, F. Ren, S. Gu, Y. Zheng, R. Zhang and J. Ye, 1.95-kV beveled-mesa NiO/β-Ga_2O_3 heterojunction diode with 98.5% conversion efficiency and over million-times overvoltage ruggedness. IEEE Transactions on Power Electronics, 37, 1223 (2021), Digital Object Identifier 10.1109/TPEL.2021.3108780

24. Jian-Sian Li, Chao-Ching Chiang, Xinyi Xia, Hsiao-Hsuan Wan, Fan Ren, S. J. Pearton; Effect of drift layer doping and NiO parameters in achieving 8.9 kV breakdown in 100 μm diameter and 4 kV/4 A in 1 mm diameter NiO/β-Ga_2O_3 rectifiers. J. Vac. Sci. Technol. A 41, 043404 (2023). https://doi.org/10.1116/6.0002722

25. F. Wu, Yuangang Wang, Guangzhong Jian, Guangwei Xu, Xuanze Zho, Wei Guo, Jiahong Du, Qi Liu, Shaobo Dun, Zhaoan Yu, Yuanjie Lv, Zhihong Feng, Shujun Cai and Shibing Long, Superior Performance β-Ga_2O_3 Junction Barrier Schottky Diodes Implementing p-NiO Heterojunction and Beveled Field Plate for Hybrid Cockcroft–Walton Voltage Multiplier, IEEE Transactions on Electron Devices, 70, 1199 (2023), doi: 10.1109/TED.2023.3239062

26. Jian-Sian Li, Hsiao-Hsuan Wan, Chao-Ching Chiang, Timothy Jinsoo Yoo, Meng-Hsun Yu, Fan Ren, Honggyu Kim, Yu-Te Lia and Stephen J. Pearton, Breakdown up to 13.5 kV in NiO/β-Ga_2O_3 vertical heterojunction rectifiers ECS J. Solid State Sci. Technol. **13,** 035003 (2024), DOI 10.1149/2162-8777/ad3457

27. Jian-Sian Li, Chao-Ching Chiang, Xinyi Xia, Hsiao-Hsuan Wan, Fan Ren and S. J. Pearton, Superior high temperature performance of 8 kV NiO/Ga_2O_3 vertical heterojunction rectifiers J. Mater. Chem. C, 11, 7750 (2023) DOI: 10.1039/D3TC01200J

28. Jian-Sian Li, Xinyi Xia, Chao-Ching Chiang, David C. Hays, Brent P. Gila, Valentin Craciun, Fan Ren, S. J. Pearton; Deposition of sputtered NiO as a p-type layer for heterojunction diodes with Ga_2O_3. J. Vac. Sci. Technol. A 41, 013405 (2023), https://doi.org/10.1116/6.0002250

29. B. Corbett, W. M. Kelly, Surface recombination in dry etched AlGaAs/GaAs double heterostructure p-i-n mesa diodes. Appl. Phys. Lett. 62, 87 (1993). https://doi.org/10.1063/1.108781

30. Jiancheng Yang, Chaker Fares, Randy Elhassani, Minghan Xian, Fan Ren, S. J. Pearton, Marko Tadjer and Akito Kuramata, Reverse Breakdown in Large Area, Field-Plated, Vertical β-Ga_2O_3 Rectifiers, ECS J. Solid State Sci. Technol. **8,** Q3159 (2019) **DOI** 10.1149/2.0211907jss

31. A. Y. Polyakov, In-Hwan Lee, N. B. Smirnov, E. B. Yakimov, I. V. Shchemerov, A. V. Chernykh, A. I. Kochkova, A. A. Vasilev, P. H. Carey, F. Ren, David J. Smith, S. J. Pearton, Defects at the surface of β-Ga_2O_3 produced by Ar plasma exposure. APL Mater. 7, 061102 (2019), https://doi.org/10.1063/1.5109025

32. Makoto Kasu, Kenji Hanada, Tomoya Moribayashi, Akihiro Hashiguchi, Takayoshi Oshima, Toshiyuki Oishi, Kimiyoshi Koshi, Kohei Sasaki, Akito Kuramata and Osamu Ueda, Relationship between crystal defects and leakage current in β-Ga_2O_3 Schottky barrier diodes, Jpn. J. Appl. Phys. 55, 1202BB (2016). https://doi.org/10.7567/JJAP.55.1202BB

33. Sayleap Sdoeung, Yuto Otsubo, Kohei Sasaki, Akito Kuramata, Makoto Kasu; Killer defect responsible for reverse leakage current in halide vapor phase epitaxial (011) β-Ga_2O_3 Schottky barrier diodes investigated via ultrahigh sensitive emission microscopy and synchrotron x-ray topography. Appl. Phys. Lett. 123, 122101 (2023). https://doi.org/10.1063/5.0170398

34. Sayleap Sdoeung, Kohei Sasaki, Katsumi Kawasaki, Jun Hirabayashi, Akito Kuramata, Toshiyuki Oishi, Makoto Kasu; Line-shaped defects: Origin of leakage current in halide vapor-phase epitaxial (001) β-Ga_2O_3 Schottky barrier diodes. Appl. Phys. Lett. 120, 122107 (2022),https://doi.org/10.1063/5.0088284

35. Z. P. Wang, N. Sun, X. X. Yu, H. H. Gong, X. L. Ji, F.-F. Ren, S. L. Gu, Y. D. Zheng, R. Zhang, A. Yu. Kuznetsov, J. D. Ye, Performance limiting inhomogeneities of defect states in ampere-class Ga_2O_3 power diodes, Appl. Phys. Rev. 11, 021413 (2024). https://doi.org/10.1063/5.0191343

36. Q. Yan, Hehe Gong, Jincheng Zhang, Jiandong Ye, Hong Zhou, Zhihong Liu, Shengrui Xu, β-Ga_2O_3 hetero-junction barrier Schottky diode with reverse leakage current modulation and

BV^2/Ron, sp value of 0.93 GW/cm^2. Appl. Phys Lett. 118, 044130 (2021). https://doi.org/10.1063/5.0044130

37. Y. Hong, X. Zheng, Y. He, H. Zhang, Z. Yuan, X. Zhang, F. Zhang, Y. Wang, X. Lu, W. Mao and X. Ma, Leakage current reduction in β-Ga_2O_3 Schottky barrier diode with p-NiOx guard ring, Appl. Phys.Lett, 12,128736(2022). https://doi.org/10.1063/5.0128736

38. Y. Lv, Y. Wang, X. Fu, S. Dun, Z. Sun, H. Liu, X. Zhou, X. Song, K. Dang, S. Liang and J. Zhang, Demonstration of β-Ga_2O_3 junction barrier Schottky diodes with a Baliga's figure of merit of 0.85 GW/cm^2 or a 5A/700 V handling capability. IEEE Transactions on Power Electronics, 36, 6179 (2020). https://doi.org/10.1109/TPEL.2020.3036442

39. Q. He, W. Hao, Q. Li, Z. Han, S. He, Q. Liu, X. Zhou, G. Xu and S. Long, β-Ga_2O_3 junction barrier Schottky diode with NiO p-well floating field rings. Chinese Physics B, 32, 128507 (2023). https://doi.org/10.1088/1674-1056/accf69

40. Advait Gilankar, Ahmad Ehteshamul Islam, Martha R. McCartney, Abishek Katta, Nabasindhu Das, David J. Smith and Nidhin Kurian Kalaricka, Three-step field-plated β-Ga_2O_3 Schottky barrier diodes and heterojunction diodes with sub-1 V turn-on and kilovolt-class breakdown, Appl. Phys. Express 17, 046501 (2024), DOI 10.35848/1882-0786/ad36ab

41. N. S. Hendricks, J. J. Piel, A. E. Islam and A. J. Green, Analytical Determination of Unipolar Diode Losses in Power Switching and Perspective for Ultra-Wide Bandgap Semiconductors, 2024 IEEE Applied Power Electronics Conference and Exposition (APEC), Long Beach, CA, USA, pp. 2670-2677 (2024), doi: 10.1109/APEC48139.2024.10509053.

42. Hehe Gong, Na Sun, Tiancheng Hu, Xinxin Yu, Matthew Porter, Zineng Yang, Fangfang Ren, Shulin Gu, Youdou Zheng, Rong Zhang, Yuhao Zhang, Jiandong Ye; Ga_2O_3/NiO junction

barrier Schottky diodes with ultra-low barrier TiN contact. Appl. Phys. Lett. 124, 233507 (2024). https://doi.org/10.1063/5.0211124

43. A. Y. Polyakov, E. B. Yakimov, D. S. Saranin, A. V. Chernykh, A. A. Vasilev, P. Gostishchev, A. I. Kochkova, L. A. Alexanyan, N. R. Matros, I. V. Shchemerov, S. J. Pearton; Trap states and carrier diffusion lengths in NiO/β-Ga_2O_3 heterojunctions. *J. Appl. Phys.* 135, 165703 (2024). https://doi.org/10.1063/5.0203526.

44. Z. P. Wang, H. H. Gong, X. X. Yu, T. C. Hu, X. L. Ji, F.-F. Ren, S. L. Gu, Y. D. Zheng, R. Zhang, J. D. Ye, Traps inhomogeneity induced conversion of Shockley–Read–Hall recombination in NiO/*β*-Ga_2O_3 p^+–n heterojunction diodes. *Appl. Phys. Lett.*122, 152102 (2023). https://doi.org/10.1063/5.0138426

45. M. Labed, N. Sengouga, C.V. Prasad, M. Henini, M., and Y.S. Rim, On the nature of majority and minority traps in β-Ga_2O_3: A review. *Materials Today Physics*, *36*, 101155 (2023).

46. Z. Zhang, Q. Song, Dinghe Liu, Yiru Yan, Hao Chen, Changgen Mu, Dazheng Chen, Qian Feng, Jincheng Zhang, Yuming Zhang, Yue Hao and Chunfu Zhang, High-quality crystalline NiO/β-Ga_2O_3 p–n heterojunctions grown by the low-cost and vacuum-free mist-CVD for device applications. *Sci. China Mater.* **67**, 1646 (2024). https://doi.org/10.1007/s40843-023-2801-2.

47. Leila Ghadbeigi, Rujun Sun, Jani Jesenovec, Arkka Bhattacharyya, John McCloy, Sriram Krishnamoorthy, Michael A. Scarpulla, Berardi Sensale-Rodriguez; Electronic and ionic conductivity in β-Ga_2O_3 single crystals, J. Appl. Phys., 131, 085102 (2022). https://doi.org/10.1063/5.0073395

48. C.V. Ramana, Swadipta Roy, Vishal Zade, Anil K. Battu, Nanthakishore Makeswaran, V. Shutthanandan, Electronic structure and chemical bonding in transition-metal-mixed Ga_2O_3

compounds, Journal of Physics and Chemistry of Solids, 157, 110174 (2021), https://doi.org/10.1016/j.jpcs.2021.110174.

49. O. Slobodyan, J. Flicker, J. Dickerson, Jonah Shoemaker, Andrew Binder, Trevor Smith, Stephen Goodnick, Robert Kaplar and Mark Hollis Analysis of the dependence of critical electric field on semiconductor bandgap, J. Materials Research 37, 849 (2022). https://doi.org/10.1557/s43578-021-00465-2

50. Gennadi Bersuker, Yongjoo Jeon, Howard R Huff, Degradation of thin oxides during electrical stress, Microelectron. Rel, 41, 1923 (2001), https://doi.org/10.1016/S0026-2714(01)00120-2.

51. National Library of Medicine, Electronegativity in the Periodic Table of Elements, https://pubchem.ncbi.nlm.nih.gov/ptable/electronegativity/

52. X. Yan, W. Li, S. M. Islam, Kasra Pourang, H. Xing, Patrick Fay and Debdeep Jena, Polarization-induced Zener tunnel diodes in GaN/InGaN/GaN heterojunctions. Appl. Phys. Lett. 107, 163504 (2015). https://doi.org/10.1063/1.4934269.

The data supporting this article have been included as part of the Supplementary Information.